

Chapter 2

Semiconductor Laser Concepts

Fundamentals of *GaAs*-based laser designs and the investigated *(In)(Ga)As* gain media concepts are discussed within this chapter. *(Al)GaAs* is the material system which is primarily employed for the infrared spectral range. Due to its versatility and ability to form dielectric mirrors for vertically emitting devices, *(Al)GaAs* forms the basis for a wide range of applications in the near infrared spectrum, and is well-established for industrial mass production.

2.1 Evolution of Semiconductor Lasers

Since its inception, some of the main goals behind semiconductor laser development have been the creation of new designs to achieve reduction of the lasing threshold, increase in modulation speed, and higher output power. Well known examples in everyday life include the *AlGaAs* laser diodes operated in *continuous-wave mode* (CW) at 780 nm employed for compact discs, and at 848 nm for laser computer mice. Optical interconnects driving the Internet rely completely on infrared semiconductor laser technology, and steady demand exists for higher modulation speeds and more cost-efficient devices. All of these examples are based on QW active media. In parallel to this quasi standard in today's industry, more sophisticated nanostructures such as QDs have been introduced as a step to improving laser performance and to unlocking new application areas. While the evolution of QD lasers started in the 1990s, the first QD devices are just now entering the market.

Lithographic techniques and chemical wet etching with subsequent overgrowth were used to fabricate the first QD lasers. These structures showed pulsed lasing at 77 K with extremely high j_{th} of 7.6 kA/cm^2 [1]. A significant advance in terms of reducing j_{th} was the use of self organized QD growth in the *Stranski-Krastanow growth mode* (SK) [2], which allowed for an essential reduction in the defect density within the QD layer. A 942 nm SK-QD laser using MBE growth was first developed by Kirstaedter et al., and demonstrated a significantly reduced j_{th} of 120 A/cm^2 at 77 K and 950 A/cm^2 at RT [3, 4]. This breakthrough started a series of reports on improved

MBE-grown SK-QD lasers with j th down to 19 A/cm^2 , realized with aluminum-oxide confinement layers and emission wavelength up to $1.3 \mu\text{m}$ [5, 6]. While the extremely low threshold characteristics and long wavelength emission around $1.3 \mu\text{m}$ of these QD lasers were predominantly achieved by MBE-grown devices (an overview can be found in [7]), the first successful MOVPE-based fabrication of SK-QD lasers emerged in 1997 [8]. Steady development of QD devices in the following years enabled success in significantly improved MOVPE-based SK-QD laser processes to close the gap to MBE devices [9, 10].

2.2 Gain Concepts

Besides $(\text{Al})\text{GaAs}$ itself, the dominant active material for GaAs -based devices are InGaAs quantization layers. Electronic states show quantization effects if at least one dimension of an enclosed nanostructure is reduced to less than the *de Broglie* wavelength of the confined charge carrier (electron: $\lambda = h/p \leq 30 \text{ nm}$). Such nanostructures of reduced dimensionality can be epitaxially grown as thin insertions within a matrix material, e.g. indium containing material can be grown as pseudomorphically strained layers. Due to the reduced band gap energy of InGaAs as compared to GaAs , electrical confinement is easily achieved. In order to fabricate customized active layers different approaches can be taken. The active layer concepts employed within devices described in this work are briefly outlined below.

2.2.1 Quantum Wells

Physically a QW is realized if a sufficiently thin layer confines charge carriers in the dimension perpendicular to its surface, while in-plane movements within the layer are possible. In contrast to bulk material, the density of states changes from a square root to a step-like function, thus the density of states becomes constant for the energy intervals between energetic eigenstates. The resulting electronic properties of such a QW can be tuned by its thickness, and are not solely dependent on material properties, such as is the case for bulk layers.

The main obstacles for highest QW quality growth are smooth interfaces [11] and dislocation free layers in heavily strained systems. Nevertheless, growth of QW in the $\text{InGaAs}/(\text{Al})\text{GaAs}$ and $\text{GaAs}/\text{AlGaAs}$ is well-established and understood. QW energy levels, optical gain, and other properties can be analytically calculated [12]. For positive values ($g_{\text{material}} \geq 0$), the material gain of a QW can be closely approximated by a logarithmic function using an empirical gain coefficient g_0 , pump current-density j , transparency current-density j_{tr} , and by neglecting saturation and occupation of excited states [13, 14].

$$g_{\text{material}} = g_0 \cdot \ln \frac{j}{j_{\text{tr}}} \quad (2.1)$$

Optical gain of a single QW is often sufficient to reach lasing threshold, whereas for high power applications or vertical designs *multi QW stacks* (MQW) can be used as active media. From the point of view of epitaxial-growth, the number of QWs and the thickness of the spacers within a MQW are limited only by the total incorporated strain. This can be partially addressed by the introduction of strain-compensating layers. Thus, the spectral tuning range of QWs is also mainly limited by strain, as maximum thickness and lattice mismatch of a grown layer are given by the accumulated elastic energy required for dislocation formation, and thus relaxation of the grown QW layer.

2.2.2 Quantum Dots

QDs confine charge carriers in all three dimensions within the length of the *de Broglie* wavelength, and the density of states in QDs is described by a δ -function instead of the step function of QWs. Consequently, they are often called zero-dimensional structures. Thus, discrete energy levels comparable to that of a single atom exist for a QD. Using the density-matrix theory Asada et al. calculated the QD gain and predicted up to ten-fold higher values for QDs as compared to equivalently thick QWs [15]. However, this advantage is limited by the fact that the occupied volume of QDs is significantly smaller than that of a QW. For a very high QD density of $1 \times 10^{11} \text{ cm}^{-2}$ and lateral QD base area of 100 nm^2 the volume is one tenth of an equally high QW. As a consequence, the overlap with the confined optical field, known as the confinement factor Γ , shrinks. Thus, the modal gain g is reduced equivalently as it is given by the product of the confinement factor and the material gain.

$$g = g_{\text{material}} \cdot \Gamma \quad (2.2)$$

The gain is also affected by the inhomogeneous broadening of the QD energy spectra to several tens of meV, caused by the size distribution of the QD ensemble. Consequently, only a part of the available QDs can contribute to the cavity mode of a laser. Additionally, finite confinement potentials render the escape of carriers into the barrier possible. An analytical description of the gain spectrum $g(\hbar\omega)$ is discussed by Bimberg et al. based on the work of Yan et al. and Chuang [16–19]. Although it is beyond the scope of the current work, profound overviews on QD properties, applications and the *Stranski-Krastanow* (SK) growth mode [2] can be found in these books: [16, 20, 21]. A theoretical model on the strain driven QD island formation has been published by Shchukin et al. [22, 23].

Currently, the basic physical mechanisms of the QD 2-D to 3-D transition after reaching a critical layer thickness of ≈ 1.7 monolayers (MLs) of *InAs* are understood [24, 25]. However, epitaxial QD growth processes are not yet able to completely control for all QD properties, such as emission wavelength and areal density independently of each other. Thus it is of fundamental interest to advance knowledge on the influence of QD growth parameters on final structural and optical QD properties.

During the overgrowth process QDs become three-dimensional inclusions within the surrounding semiconductor matrix crystal. But in contrast to QW epitaxy, which shows always a flat growth front, all QD layer overgrowth processes start with a three dimensionally shaped, and thus *rough* surface, which needs to be flattened during spacer growth prior to the following QD layer being grown. In consequence, advanced growth processes are necessary to deal with this challenge.

As previously mentioned, the inherent QD size distribution as a result of the self-organized SK process causes QD layers to show a much broader luminescence when compared to QWs. Thus, the peak gain per QD layer is lower than for QWs, and QD stacking is often required. Whereas the broad spectral gain width can be used to provide a unique advantage for QD-based VECSELs, as is shown in Chap. 6. Another intrinsic advantage of QDs is the very widely accessible spectral range. A single material system such as *InGaAs/GaAs* enables the fabrication of lasers for the entire wavelength range from $\approx 1000\text{ nm}$ up to $\approx 1350\text{ nm}$ by tuning QD growth parameters.

2.2.3 Sub-Monolayer Structures

In contrast to QWs and QDs, research on SML structures as active media is rather young. Comprehensive reviews on SML self-organization, optical properties, and applications have been published by Krestnikov et al. and Ledentsov et al. [27, 28]. SML structures consist of a superlattice of SML depositions of low band-gap material separated by few MLs of thick matrix material spacer layers. All iterated SML depositions consist of less material than is needed to form a complete ML on the surface. Thus, the initial SML deposition is obliged to form islands where the size of these SML islands is defined by the minimization of the total energy of the system. While the surface energy component depends only on the amount of deposited material, the boundary and strain energies depend on the island size [29, 27]. For all subsequently iterated SML depositions the term $E_{\text{strain}}^{\text{interaction}}$ is additionally applied for the elastic energy resulting from the interaction of surface islands with buried islands, leading to correlations and anti-correlations within the SML structure [30]. While a single SML island is too small to confine an electron, the close correlation of these *InAs* islands in the vertical plane upon stacking ultimately leads to the formation of a three-dimensional structure capable of acting as a QD within the crystal (cf. schematic Fig. 2.1).

Theoretical models can explain the physics of SML formation and SML wave-functions, however, an understanding of epitaxial growth processes and their parameters in controlling SML optical characteristics is in the early stages. Structural investigations and optical characterization of MBE-grown *InGaAs/GaAs* SMLs describe the fabricated structures as a mixed state of QDs enclosed within a QW showing distinct QD properties, which are overlapped by the stronger QW luminescence at higher excitation levels [31, 32]. MOVPE-grown SML structures described in this work use nominally the same amount of 0.5 ML *InAs* per SML

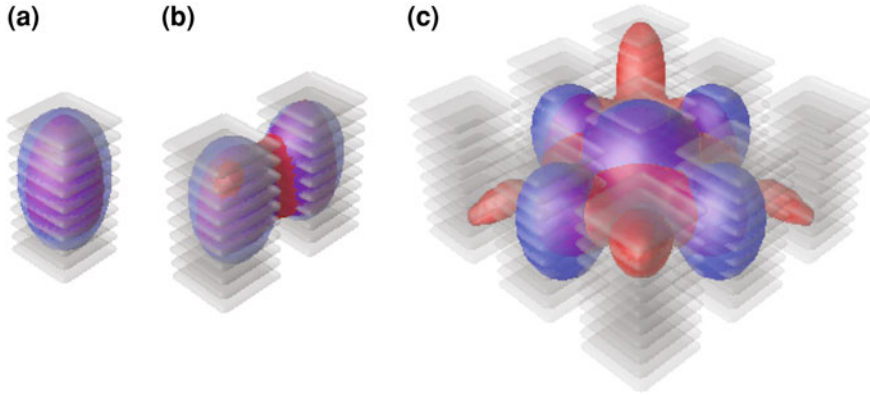


Fig. 2.1 Schematic of the lateral coupling of *InAs*/*GaAs* SML structures based on calculations of electron (blue) and hole (red) wave-functions by Dr. Andrei Schliwa. In the vertical plane *InAs* islands are separated by 3 ML *GaAs*, laterally a distance of 2 nm is set. **a** Isolated 10-fold SML structure. **b** A pair of SML structures shows lateral coupling. **c** Wave functions extend laterally across the 3×3 SML configuration

deposition cycle as in the cited references, however the optical properties are dominated by QW-like characteristics. A theoretical assessment predicts an intended ultra-high SML island density of $\approx 10^{12} \text{ cm}^{-2}$, and an average distance between these *InAs* islands of only 2 nm for this amount of material. This narrow lateral separation allows for lateral electronic coupling between neighboring SML island stacks, leading to optical properties at high excitations which are comparable to very rough QWs [33]. A schematic representation based on calculations by Andrei Schliwa is given in figure depicting the coupling of neighboring SML stacks Fig. 2.1. Investigations of our samples by *cross sectional scanning tunneling microscopy* (XSTM) confirmed the predicted narrow separation between adjacent *InAs*-rich agglomerations as shown in Fig. 2.2. Individual SML depositions are not resolved in the XSTM picture of this SML structure due to the very thin spacing of 1.5 ML *GaAs*, and the indium segregation in the growth direction. Detailed results from these SML investigations by XSTM are published in [26]. Similar SML structures are used as active media for the SML VECSELs presented in Chap. 6.

2.3 Semiconductor Laser Basics

All modern SCH-semiconductor laser designs have to achieve both confining photons, and confining charge carriers according to their respective wavelengths. In order to confine photons, the typical thickness of a cavity extends to a few hundred nanometers on the order of $\approx \lambda/n$ while electrons require nanostructures with dimensions about one order of magnitude smaller according to the *de-Broglie* wavelength

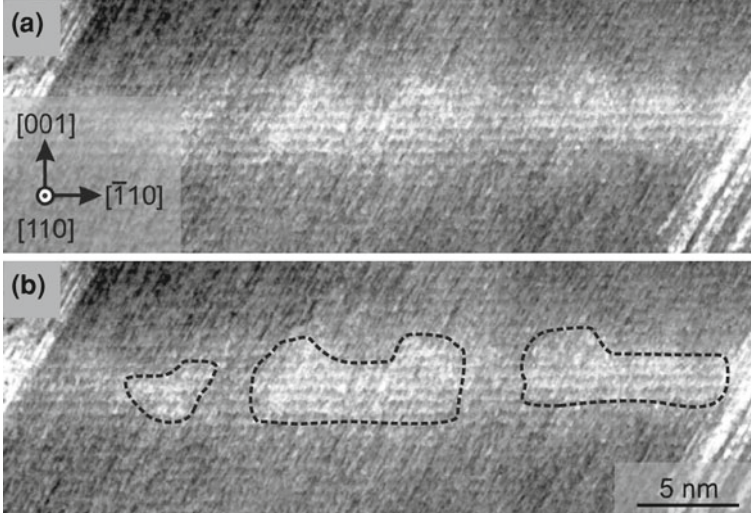


Fig. 2.2 **a** and **b** are identical XSTM images, in **b** *InAs*-rich agglomerations are indicated by dashed lines as a guide to the eye. Close-view filled-state XSTM images of a 10-fold SML stack with 0.5 ML *InAs* and 1.5 ML *GaAs* spacers per iteration, taken at 110 cleavage surface using $V_S = -2.6$ V and $I_T = 60$ pA. This work has been published in [26]

$\lambda = h/p$. Thus, it is crucial to position nanostructures at the maximum of the confined optical field for optimum modal gain (cf. Eq. 2.2). The lasing threshold is achieved if the modal gain equals the internal losses α_i plus the mirror losses α_{mirror} of the laser. With mirror reflectivity R_x and cavity length L this can be written as:

$$g(j_{th}) = \alpha_i + \alpha_{mirror} = \alpha_i + \frac{1}{2L} \ln \left(\frac{1}{R_1 R_2} \right) \quad (2.3)$$

Using Eqs. 2.1 and 2.2 the threshold current-density j_{th} can be written as:

$$j_{th} = j_{tr} \cdot \exp \left(\frac{\alpha_i}{\Gamma g_0} + \frac{1}{\Gamma g_0} \cdot \frac{1}{2L} \ln \left(\frac{1}{R_1 R_2} \right) \right) \quad (2.4)$$

The transparency current density is the current density which renders the laser neither optically absorbing, nor optically amplifying; thus the laser is transparent. To experimentally determine gain values and transparency current density j_{tr} of edge emitters, several edge-emitters of different lengths were cleaved to enable the measurement of a set of lasers with different cavity lengths. By interpolating the threshold current density j_{th} values of the measured devices to infinite cavity length, the transparency current density can be directly determined from the following Eq. 2.4:

$$j_{tr} = \frac{j_{th}(L = \infty)}{\exp\left(\frac{\alpha_i}{\Gamma_{g0}}\right)} \quad (2.5)$$

Another important laser parameter is the internal quantum efficiency η_{int} , which is defined as the ratio of the internally-emitted photons to electron-hole pairs injected into the p-n junction of the laser diode. In the experiment, only the out-coupled photons, which are equivalent to the mirror losses α_{mirror} , can be measured. The ratio of the out-coupled photons to the injected electron-hole pairs is defined as differential quantum efficiency η_{diff} :

$$\eta_{diff} = \eta_{int} \cdot \frac{\alpha_{mirror}}{\alpha_{mirror} + \alpha_i} \quad (2.6)$$

Experimentally η_{diff} is deduced from the linear slope of the optical output power as a function of the pump current above the lasing threshold:

$$\eta_{diff} = \frac{\Delta P}{\Delta I} \cdot \frac{e}{h\nu} \quad (2.7)$$

Measured η_{diff} values for lasers with different cavity lengths can then subsequently be used to determine η_{int} and α_i . Using the Eq. 2.6 and the definition of the mirror losses from Eq. 2.3 $1/\eta_{diff}$, this can be written as:

$$\frac{1}{\eta_{diff}} = \frac{1}{\eta_{int}} - \left(\frac{1}{\ln(R_1 R_2)} \cdot \frac{2\alpha_i}{\eta_{int}} \right) \cdot L \quad (2.8)$$

Now $1/\eta_{diff}$ can be drawn as a function of L and linearly fitted, this directly gives for $L = 0$ a value for $1/\eta_{int}$ and allows use of the slope to calculate α_i .

Aside from using their fundamental physical device properties, semiconductor lasers can be assigned to two distinct groups:

- **Edge-emitting lasers:** Light within the cavity propagates parallel to the semiconductor wafer surfaces, and thus also parallel to all epitaxial grown layers. Cleaved wafer facets are used to reflect and/or couple out laser light. Device cavities of several mm in length can be fabricated due to light propagation along the active zone in order to increase total gain.
- **Surface-emitting lasers:** The cavity axis is perpendicular to the semiconductor wafer surface and light is coupled out through the epitaxial surface or the bottom of the wafer. As light propagation is also perpendicular to the active layers, the pumped active area and the achievable number of grown active layers limit output powers.

In addition to this fundamental classification, a multitude of application-specific designs exist to generate appropriate device characteristics. For all theoretical concepts the design inherently defines the maximal laser properties which are attainable. Subsequently, growth and processing expertise need to attain the given intrinsic

optimum e.g. by achieving maximum gain, eliminating defects, and providing sufficient cooling. In the following, the basic characteristics, possibilities, and limits for the fabricated lasers described within this work are discussed.

2.3.1 Edge-Emitting Lasers

For all edge-emitting lasers light propagation is in-plane, as epitaxial processes offer only vertical structuring, additional lateral confinement is required. While the vertical confinement is realized by epitaxially grown cladding layers with a lower refractive index, the lateral confinement is set up post-growth by etching stripes into the wafer surface. In this manner, index guiding in the vertical and lateral directions is achieved (gain guiding concepts are also possible). However, as the vertical extension of the waveguide is significantly smaller than the processed lateral extension, the asymmetric beam shape limits coupling capabilities to optical fibers. A current guiding effect is also realized by the etching of the top-cladding layer, which is limited by the fact that charge carriers can still diffuse laterally within the waveguide. By simply using cleaved facets as perfectly plane-parallel mirrors to form the resonator, no epitaxial or subsequently processed mirrors are required for laser operation. Many variants of this basic edge-emitter concept exist to enable specific features, such as single-mode operation by small ridge widths of only a few microns, or frequency selectivity by a distributed feedback laser design.

Horizontally emitting lasers within this work are solely broad-waveguide edge-emitters. This simple variant requires a minimized processing effort, enabling fast laser parameter feedback times (< 2 days) for the development of epitaxial processes as detailed in Sect. A.5.1. However, these lasers are multimode devices that are not optimized for highest performance, but instead offer a valuable assessment of the epitaxial process quality. By cleaving the laser stripes as the last step of processing, different cavity lengths can be easily created in order to assess relevant characteristic laser parameters.

2.3.2 Surface-Emitting Lasers

In contrast to horizontally-emitting devices, all vertical-emitting designs require additional mirrors which are either epitaxially grown or externally mounted, or are added during processing. The biggest advantage to the vertical concepts is the possibility of a circular geometry, enabling a higher laser beam quality due to the resulting circular beam shape.

EOM VCSEL

The very short cavity length of a VCSEL ($<1\text{ }\mu\text{m}$) limits the modal gain and causes the mirror losses α_{mirror} to be the dominant optical loss factor (cf. Eq. 2.3) for the VCSEL concept. Consequently, VCSELs require mirror reflectivity from both facets well above 99 %, to enable reasonable threshold current-density levels. Such reflectivity levels are mostly realized by thick *distributed Bragg reflectors* (DBRs) with at least 20 pairs in the *AlAs/GaAs* system. Optical confinement for VCSEL is achieved by etching a circular mesa into the epitaxial structure to enable index guiding and charge-carrier confinement. In order to improve laser characteristics, an oxide aperture layer is often added to confine the applied current to the mesa center, to reduce leakage currents, and for mode selection. As electrically pumped VCSEL use, in most cases, a circular top contact surrounding the output mirror, the maximum output power is limited to milliwatt levels by the area, which can be homogeneously pumped. As soon as contacts are processed VCSELs can easily be tested on wafer without any device separation, due to the fact that light is emitted from the surface.

In this work a more complex variant of the VCSEL is realized, the EOM VCSEL, which includes a monolithically integrated modulator within a second cavity. To access the modulator section, conventional VCSEL processing is altered to realize a third circular middle contact. The same restrictions and advantages as those mentioned above apply to the EOM VCSEL design.

VECSEL

In contrast to all other laser designs within this work, VECSEL are usually optically pumped, and no lateral patterning or processing of the wafer is applied to the structure post-growth. Instead, the optically-irradiated area defines the actively pumped region of the laser, thus confining the charge-carrier generation to an almost circular spot. For optimum performance, this pump spot should match the focus diameter of the external mirror, which defines the diameter of the laser within the gain chip. In comparison to VCSEL designs, this VECSEL diameter can be much larger—up to hundreds of microns—and the active part of the cavity can be extended to more than a micron, depending on the pump laser absorption characteristics. In consequence, VECSELs enable very high output-power levels of up to several watts in CW mode. VECSEL limitations are given by the almost non-existent lateral confinement and the complex setup, requiring an external pump laser and optical alignment upon mounting the gain chip to an elaborate heat sink. In contrast to other monolithic designs, this external cavity design enables easy intra-cavity access e.g. for efficient frequency doubling. Thus, complete VECSELs are much larger than edge-emitters or VCSELs but offer flexibility, high brilliance and high power.

References

1. H. Hirayama, K. Matsunaga, M. Asada, Y. Suematsu, Lasing action of Ga_{0.67}In_{0.33}As/GaInAsP/InP tensile-strained quantum-box laser. *Electron. Lett.* **30**(2), 142 (1994). ISSN 00135194
2. I.N. Stranski, L. Krastanow, Zur theorie der orientierten Ausscheidung von Ionenkristallen aufeinander. *Monatshefte für Chemie/Chem. Mon.* **71**, 351 (1938). ISSN 0026-9247
3. N.N. Ledentsov, V.M. Ustinov, A.Y. Egorov, M.V. Zhukov, A.E. Maximov, I.G. Tabatadze, P.S. Kop'ev, Optical properties of heterostructures with InGaAs-GaAs quantum clusters. *Fiz. i Tekh. Poluprovodn.* **28**, 1484 (1994)
4. N. Kirstaedter, N. Ledentsov, M. Grundmann, V. Bimberg, D. Ustinov, S. Ruvimov, M. Maximov, P. Kop'ev, Z. Alferov, U. Richter, P. Werner, U. Gösele, J. Heydenreich, Low threshold, large T_0 injection laser emission from (InGa)As quantumdots. *El. Lett.* **30**(17), 1416 (1994)
5. L.F. Lester, A. Stintz, H. Li, T.C. Newell, E.A. Pease, B.A. Fuchs, K.J. Malloy, Optical characteristics of 1.24 μ m InAs quantum-dot laser diodes. *IEEE Photonics Technol. Lett.* **11**(8), 931 (1999). ISSN 1041-1135
6. G. Park, O. Shchekin, D. Huffaker, D. Deppe, Low-threshold oxide-confined 1.3- μ m quantum-dot laser. *IEEE Photonics Technol. Lett.* **12**(3), 230 (2000). ISSN 10411135
7. I. Kaiander, *MOCVD growth of InGaAs/GaAs QDs for long wavelength lasers and VCSELs*, Dissertation, Technische Universität Berlin, 2006
8. F. Heinrichsdorff, M.-H. Mao, N. Kirstaedter, A. Krost, D. Bimberg, A.O. Kosogov, P. Werner, Room-temperature continuous-wave lasing from stacked InAs/GaAs quantum dots grown by metalorganic chemical vapor deposition. *Appl. Phys. Lett.* **71**(1), 22 (1997)
9. I.N. Kaiander, R.L. Sellin, T. Kettler, N.N. Ledentsov, D. Bimberg, N.D. Zakharov, P. Werner, 1.24 μ m InGaAs/GaAs quantum dot laser grown by metalorganic chemical vapor deposition using tertiarybutylarsine. *Appl. Phys. Lett.* **84**(16), 2992 (2004). ISSN 00036951
10. A. Strittmatter, T.D. Germann, T. Kettler, K. Posilovic, U.W. Pohl, D. Bimberg, Alternative precursor metal-organic chemical vapor deposition of InGaAs/GaAs quantum dot laser diodes with ultralow threshold at 1.25 μ m. *Appl. Phys. Lett.* **88**(26), 262104 (2006)
11. D. Bimberg, F. Heinrichsdorff, R.K. Bauer, D. Gerthsen, D. Stenkamp, D.E. Mars, J.N. Miller, Binary AlAs/GaAs versus ternary GaAlAs/GaAs interfaces: a dramatic difference of perfection. *J. Vac. Sci. Technol. B* **10**(4), 1793 (1992)
12. T. Makino, Analytical formulas for the optical gain of quantum wells. *IEEE J. Quantum Electron.* **32**(3), 493 (1996). ISSN 00189197
13. L. Coldren, S. Corzine, *Diode Lasers and Photonic Integrated Circuits* (Wiley, New York, 1995)
14. F. Bachmann, P. Loosen, R. Proprawe, *High-Power Diode Lasers Technology and Applications* (Springer Science and Business Media, New York, 2007)
15. M. Asada, Y. Miyamoto, Y. Suematsu, Gain and the threshold of three-dimensional quantum-box lasers. *IEEE J. Quantum Electron.* **22**(9), 1915 (1986). ISSN 0018-9197
16. D. Bimberg, M. Grundmann, N.N. Ledentsov, *Quantum Dot Heterostructures* (Wiley, Chichester, 1998)
17. R. Yan, S. Corzine, L. Coldren, I. Suemune, Corrections to the expression for gain in GaAs. *IEEE J. Quantum Electron.* **26**(2), 213 (1990). ISSN 00189197
18. S.L. Chuang, *Physics of Optoelectronic Devices*, 2nd edn. (Wiley, New York, 2009). ISBN 978-0-470-29319-5
19. L.V. Asryan, M. Grundmann, N.N. Ledentsov, O. Stier, R.A. Suris, D. Bimberg, Maximum modal gain of a self-assembled InAs/GaAs quantum-dot laser. *J. Appl. Phys.* **90**(3), 1666 (2001). ISSN 00218979
20. M. Grundmann (ed.), *Nano-Optoelectronics* (Springer, Berlin, 2002)
21. D. Bimberg (ed.), *Semiconductor Nanostructures* (Springer, Berlin, 2008)
22. V.A. Shchukin, N.N. Ledentsov, P.S. Kop'ev, D. Bimberg, Spontaneous ordering of arrays of coherent strained Islands. *Phys. Rev. Lett.* **75**(16), 2968 (1995)

23. V. Shchukin, D. Bimberg, Strain-driven self-organization of nanostructures on semiconductor surfaces, *Appl. Phys. A: Mater. Sci. Process.* **67**, 687 (1998). ISSN 0947-8396
24. D. Leonard, K. Pond, P. Petroff, Critical layer thickness for self-assembled InAs Islands on GaAs. *Phys. Rev. B* **50**(16), 11687 (1994). ISSN 0163-1829
25. F. Heinrichsdorff, *MOCVD growth and laser applications of In(Ga)As/GaAs Quantum Dots*, Dissertation, Technische Universität Berlin, 1998
26. A. Lenz, H. Eisele, J. Becker, J.-H. Schulze, T.D. Germann, F. Luckert, K. Pötschke, E. Lenz, L. Ivanova, A. Strittmatter, D. Bimberg, U.W. Pohl, M. Dähne, Atomic structure and optical properties of InAs submonolayer depositions in GaAs. *J. Vac. Sci. Technol. B* **29**(4), 04D104 (2011). ISSN 10711023
27. I. Krestnikov, N. Ledentsov, A. Hoffmann, D. Bimberg, Arrays of two-dimensional Islands formed by submonolayer insertions: growth, properties, devices. *Physica Status Solidi(a)* **183**(2), 207 (2001). ISSN 0031-8965
28. N.N. Ledentsov, D. Bimberg, F. Hopfer, A. Mutig, V.A. Shchukin, A.V. Savel'ev, G. Fiol, E. Stock, H. Eisele, M. Dähne, D. Gerthsen, U. Fischer, D. Litvinov, A. Rosenauer, S.S. Mikhlin, A.R. Kovsh, N.D. Zakharov, P. Werner. Submonolayer quantum dots for high speed surface emitting lasers. *Nanoscale Res. Lett.* **2**(9), 417 (2007). ISSN 1931-7573
29. V. Shchukin D. Bimberg, Spontaneous ordering of nanostructures on crystal surfaces. *Rev. Mod. Phys.* **71**(4), 1125 (1999). ISSN 0034-6861
30. V. Shchukin, D. Bimberg, V. Malyshev, N. Ledentsov, Vertical correlations and anticorrelations in multisheet arrays of two-dimensional Islands. *Phys. Rev. B* **57**(19), 12262 (1998). ISSN 0163-1829
31. Z. Xu, D. Birkedal, J.M. Hvam, Z. Zhao, Y. Liu, K. Yang, A. Kanjilal, J. Sadowski, Structure and optical anisotropy of vertically correlated submonolayer InAs/GaAs quantum dots. *Appl. Phys. Lett.* **82**(22), 3859 (2003). ISSN 00036951
32. Z. Xu, K. Leosson, D. Birkedal, V. Lyssenko, J.M. Hvam, J. Sadowski, InGaAs/GaAs quantum-dot-quantum-well heterostructure formed by submonolayer deposition. *Nanotechnology* **14**(12), 1259 (2003). ISSN 0957-4484
33. Z. Xu, Y. Zhang, J.M. Hvam, J. Xu, X. Chen, W. Lu, Carrier dynamics in submonolayer InGaAs/GaAs quantum dots. *Appl. Phys. Lett.* **89**(1), 013113 (2006). ISSN 00036951



<http://www.springer.com/978-3-642-34078-9>

Design and Realization of Novel GaAs Based Laser
Concepts

Germann, T.D.

2012, XIII, 150 p., Hardcover

ISBN: 978-3-642-34078-9